Advances in Nano Research, *Vol. 11, No. 1 (2021) 101-113*
https://doi.org/10.12989/anr.2021.11.1.101

Assessment of microstructure and surface effects on vibrational characteristics of public transportation

Abdulmajeed S. Alsultan*

Prince Sattam Bin Abdulaziz University, College of Engineering, Department of Civil Engineering, Alkharj, 16273, Saudi Arabia

(*Received January 4, 2020, Revised June 6, 2021, Accepted June 29, 2021*)

Abstract. This study analyzes the influence of surface effects on transportation vibrational properties. The evaluation of vibration impacts was done in accordance with the standards laid out in ISO 2631-1 for convenience on public transport (bus). The QCM (Quarter Car Model) with a quarter vehicle mass and variable was evaluated on exchange force between paving and three vehicle typologies (car, bus, and truck) using Matlab. The driver's, passengers in the center section, and passengers in the rear overhang's comfort is evaluated. The ten-degree oscillatory bus model has been designed for analytical requirements. First, the vibration propagation effects of different bus types are examined. Numerical methods are next briefly addressed to vibration propagation modeling inside the path and in the soil. Then a detailed discussion on the development of numerical models with an examination of the appropriateness of various modeling techniques for vehicle impact analysis will be given. Bus excitation has been created by using the asphalt-concrete road roughness power-spectral density as stated in the H. Braun model. This article illustrates how this dynamic overcharge might be predetermined according to the deterioration of the pavements' surface. This is a valuable resource for the design and maintenance of road pavements.

Keywords: microstructure; surface effects; transportation; vibrational characteristics

1. Introduction

Surface phenomena are increasingly essential for many innovative micro-Nano devices and applications, since the sizes and the surface-to-volume ratios between these devices are tiny (Hu *et al*. 2020, Yang *et al*. 2020, Hong *et al*. 2021, Shao *et al*. 2021). Surfaces are often proportional to their surface intensity (e.g., adhesion and friction) and hence are scaled as the second force of a typical device length, whereas volume forces (e.g., inertia) tend to be the third power of the characteristic length (Zhang *et al*. 2019, Ji *et al*. 2020a, Ni *et al*. 2021, Zhang *et al*. 2021). Thus, surface effects are dominant at micro/nanometer scales, but the volume effects are insignificant (Kazerani *et al*. 2014, Fanaie and Shamlou 2015, Hajilak *et al*. 2019). The macro, micro and nanoscale common definitions are the following. The microscale is commonly referred to as the length scale in the region from 1 mm to 100 nm, whereas the length scale is named the nanoscale from 100 nm up to 1 nm (Wang *et al*. 2018, Zhang *et al*. 2020, 2021, Zhu *et al*. 2021). The macroscale is a longitudinal scale more than 1 mm while the atomic scale is a length less than 1 nm. Recent micro/Nano technological developments have enabled the construction of micro/Nano-structured functional surface systems with low adhesion micro/Nano topography (Yin *et al*. 2015, Ji *et al*. 2020b, Hou *et al*. 2021, Qiao *et al*. 2021). Surface topography is defined by variations in roughness, porosity etc. from a completely flat plane (Ebrahimi *et al*. 2019, Chen *et al*. 2020, Yang *et al*. 2020b). For example, super hydrophobic (lotus effect) surfaces that are very water-repellent and gecko effect surfaces display regulated adhesion through their micro/Nano surface topography (Xu *et al*. 2014, Qi and Fourie 2019, Qi *et al*. 2020). Many of these surfaces are inspired by living materials and surfaces dubbed biomimetic surfaces (Shah *et al*. 2016a, Zandi *et al*. 2018, Naghipour *et al*. 2020, Yazdani *et al*. 2020, Rajaei *et al*. 2021). Advances in Nanotechnology have made it possible to build materials that demonstrate greater performance, durability, and sustainability than ordinary concrete and alloys such as composites and metal matrix composites (Shah *et al*. 2015, 2016b, Nosrati *et al*. 2018, Toghroli *et al*. 2018, Ziaei-Nia *et al*. 2018). In a region such as Milwaukee in Wisconsin, which is a hub of the fresh water industry owing to its proximity to the Great Lakes and the diversity of businesses connected to water, functional surfaces for water and ice applications are of special importance (Mohammadhassani *et al*. 2014a, Tahmasb *et al*. 2016, Wei *et al*. 2018, Li *et al*. 2019, Luo *et al*. 2019). The water industry has common raw materials for metals (such as steel, brass and cast iron) (Daie *et al*. 2011, Mohammadhassani *et al*. 2014c, Nasrollahi *et al*. 2018, Paknahad *et al*. 2018). The average snowfall in Milwaukee is 133 cm a year due to both the lake effect and the latitude to the north. The salt used for ice and snow removal is corrosive and can harm metal components such as automotive components, metal reinforcements, or water pipes' longevity and efficiency (Hamidian *et al*. 2011, Shah *et al*. 2016b, Shahabi *et al*. 2016, Heydari and Shariati

*Corresponding author, Ph.D.,
E-mail: asalsultan@psau.edu.sa

ISSN: 2287-237X (Print), 2287-2388 (Online)

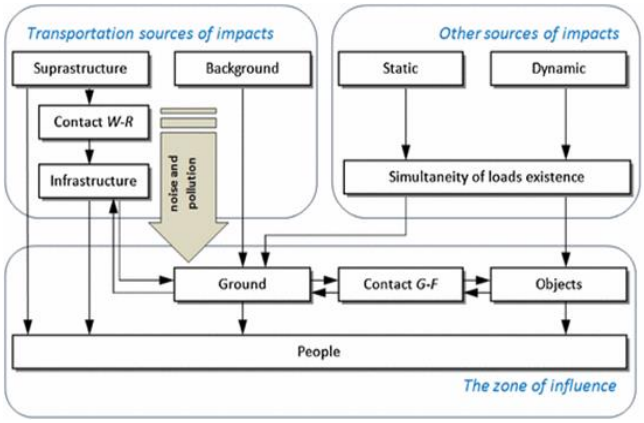

Fig. 1 Sources of impacts, interaction points, and flow directions of dynamic enforcement signal

2018, Paknahad *et al*. 2018). It is vital that fundamental features of how micro/Nano topography has an effect on the surface characteristics at the macroscale are examined in order to comprehend the structure-perfect link between these new materials and surfaces (Khorramian *et al*. 2016, Hosseinpour *et al*. 2018, Safa *et al*. 2019, Afshar *et al*. 2020, Naghipour *et al*. 2020b). The topography of the surface micro/Nano can be seen as a mixture of spatial models, while rapid vibrational tiny amplitudes provide periodic temporal motives (Arabnejad Khanouki *et al*. 2016, Khorami *et al*. 2017, Suhatril *et al*. 2019, Trung *et al*. 2019b, Toghroli *et al*. 2020). A vibration is thought to be rapid or sluggish when compared to the physical system's inherent oscillations (Sinaei *et al*. 2012, Khorramian *et al*. 2017, Toghroli *et al*. 2017, Milovancevic *et al*. 2019, Sajedi and Shariati 2019). The vibration frequency is considerably higher than the natural oscillation frequency of the system (Arabnejad Khanouki *et al*. 2010, Sinaei *et al*. 2011, Jalali *et al*. 2012, Ismail *et al*. 2018, Davoodnabi *et al*. 2019). The movement separation technique is a mathematical tool used for the study of the dynamics of stiff bodies in fast-paced areas (Mohammadhassani *et al*. 2013, Toghroli *et al*. 2014, 2016, Mansouri *et al*. 2019). The quick vibrations can be replaced with an effective force using this approach (Sadeghipour Chahnasir *et al*. 2018, Sedghi *et al*. 2018, Katebi *et al*. 2019, Safa *et al*. 2020). This effective strength is achieved by averaging the vibrations throughout time (Mohammadhassani *et al*. 2014b, Goudarzi *et al*. 2016, Safa *et al*. 2016, Fanaie *et al*. 2017, Trung *et al*. 2019a). The vibration-induced stability of an inverted pendulum is the simplest mechanical example of a vibration manifesting as an efficient power (Ghabussi *et al*. 2019, Habibi *et al*. 2019, Pourjabari *et al*. 2019, Safarpour *et al*. 2019, Ebrahimi *et al*. 2020). A strong methodology for studying the influence of tiny patterns on the macroscopic status or characteristics of a system offers a way of separating motion (Habibi *et al*. 2020, Shariati *et al*. 2020, Al-Furjan *et al*. 2021, Zhao *et al*. 2021). Due to similarities in the effects of small amplitude patterns and small rapid vibrations, this approach can be applied in the areas of surface technology, physical chemistry and materials research. Fig. 1 shows the sources of impacts, interaction points, and flow directions of dynamic enforcement signals.

During a vehicle ride, drivers and passers-by are exposed to road surface vibrations (Fanaie and Tahriri 2017, Afsar Dizaj *et al*. 2018, Dong *et al*. 2018, Tan *et al*. 2021). Vibration causes pain, reduces work capacity and can impact health over longer periods of time (Mladenovic 1999, Dedovic´ 2004, Moghadam *et al*. 2010, Fanaie *et al*. 2012, 2019). Building machinery, agriculture, lorries and bus drivers are among the most hazardous groups (Kompier 1996). Studies (Kompier 1996, Okunribido *et al*. 2007, Picu 2009) have revealed that bus drivers are subjected to vibrations of high intensity. Long-term exposure to high-level vibrations causes drivers to experience a variety of health issues, such as muscular skeletal diseases (low-back pain, neck, shoulder, and knee discomfort), mental disorders (tiredness, strain, mental weariness), sleep disturbance, and so on (Whitelegg and Cross 1995, Alperovitch-Najenson *et al*. 2010, Huang *et al*. 2021a, Jiao *et al*. 2021, Ma *et al*. 2021). The European Union enacted Directive 2002/44 on 25 June 2002 with a view of reducing harmful effects on vibration and ensuring health at work. It specifies permissible exposure limit (threshold) values for entire body vibrations at work and clearly emphasizes employers' need to implement adequate safety measures in line with these levels (Nelson and Brereton 2005, Najarkolaie *et al*. 2017, Ghanbari-Ghazijahani *et al*. 2020, Rezaeian *et al*. 2020). Timely action for both drivers and passengers to prevent vibration damage involves ongoing monitoring of the degree of vibration (Asadolahi and Fanaie 2020, Partovi and Fanaie 2020, Razavian *et al*. 2020, Mehrabi *et al*. 2021). This frequently implies measuring the degree of exposure to vibration in users under real-life circumstances. In recent years, vibration tests have not only been done in the vehicle to evaluate its oscillatory comfort under real conditions (Fig. 3), but also to evaluate the suspension system in the dumping of vibrations transferred from the vehicle's wheels to the vehicle's body. In (Litak *et al*. 2009), the vertical acceleration signals were recorded during passage through the railway cross in the suspension system of the delivery truck. In the dampening of shock vibrations transferred from the railway crossing to the vehicles suspended mass, it was possible to assess the quality of the suspension system by measuring the acceleration. The analysis of recorded vertical acceleration in the vehicle suspension system in revealed that the suspension system is more efficient at dampening higher-frequency vibration levels for three different types of excitations (asphalt, sett, and rail cross) (Borowiec *et al*. 2010). In addition to the observations, simulations utilizing the model oscillator (Pečeliūnas *et al*. 2003, 2005) can be carried out for examination. When measurements are rarely carried out due to different restrictions, simulations take more relevance. The incorporation of previously observed traffic rarity into the oscillatory (Pečeliūnas *et al*. 2005), the previously observed traffic rarity is a quality study of the oscillatory behavior of vehicles. In this article, the bus excitement was modeled using the Power Spectral Density of asphalt-concrete road roughness in very excellent condition, since it was difficult to carry out an actual screening of road roughness. Here, a spatial oscillatory model of the intercity bus IK-301 with 10

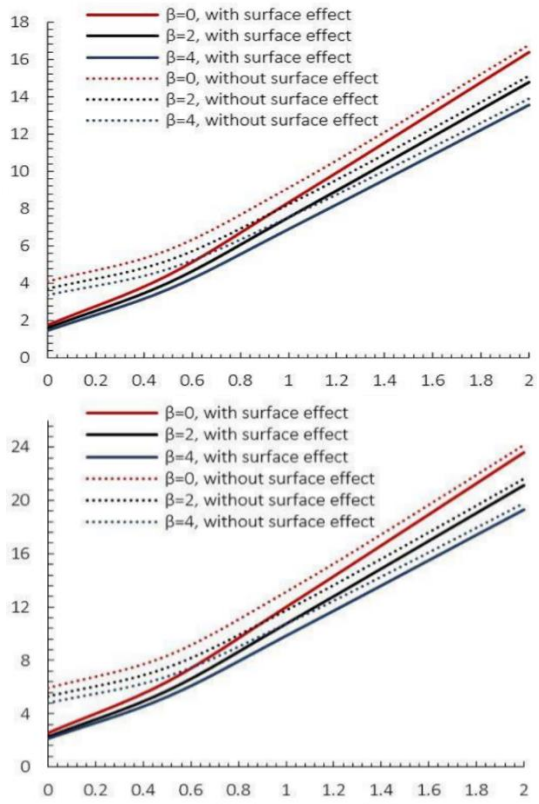

Fig. 2 Variation of dimensionless frequency of NL-CS FG versus length scale parameter for various nonlocal parameters (L/h = 40, p = 0.5)

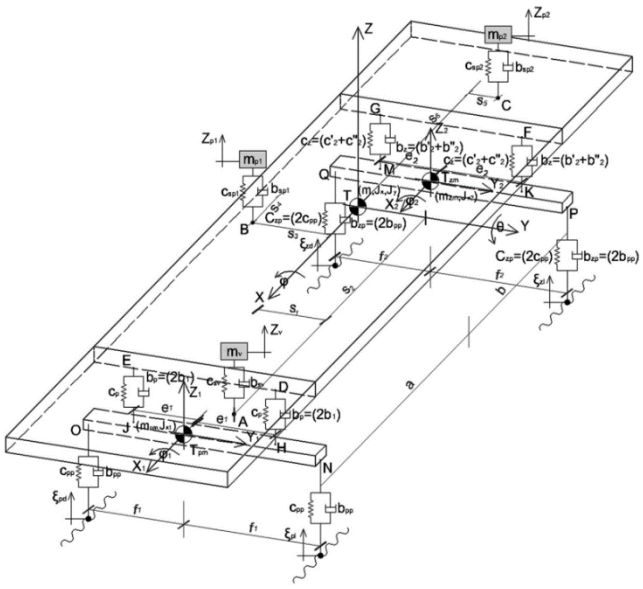

Fig. 3 Oscillatory model of the bus IK-301

degrees of freedom was applied for the investigation of user oscillatory comfort. The oscillating comfort of the driver and passenger was measured in accordance with the process and criteria outlined in the ISO 2631-1 standard of 1997 (2631 1997). In line with ISO 2631-1 of 1978, it has also been established here that drivers can have the permissible exposure time for the decreased comfort criterion. The impact of the shock and shipment vibration might lead to severe damage to the goods say fresh products (fruits and vegetables). The shipping and handling of fresh fruits and vegetables can lead to different types of contusions and cuts that jeopardize their quality, esthetic appeal and diminish their economic worth for both growers and retails. In today's expanding international trade, there are numerous modes of transportation that necessitate intermodal transit via land, sea, and air. Trucks remain, nonetheless, the most anticipated form of delivery of perishable materials like fresh produce for surface transit and time-sensitive distribution. This is partly because trucks are usually utilized as the initial means of delivery from the farm or packing plant to the department stores (Fig. 6). Therefore, distribution data is an important component in the design of optimal packaging solutions. The dynamic levels observed in actual shipments may also be utilized to build test techniques for the simulation of the transportation environment and for the prevention of product loss or sales value. The primary goal of this study was to monitor and evaluate distribution measurements focusing on key fresh product areas at retail distributors and, later, in retail outlets. Furthermore, the recorded vibration levels were compared to vibration data utilized for vehicle transit in Western nations. Fig. 2 shows the fluctuation of the NL-CS FG dimensionless frequency against the parameter length scale of the several non-local parameters (L/h = 40, p = 0.5).

1.1 Bus oscillatory model

The IK-301 bus uses a steep axle suspension system. The front axle is connected to the body with two air bags and with four telescopic shock absorbers (RABA/A 932.10), while the rear axle, with four air bags and 4 telescope shock absorbers, and is connected to the bottom of the air (RABA /A 109.29). The bus features two front axle wheels and four rear axle wheels. The spatial model of the IK-301 bus with 10 degrees of freedom is presented in Fig. 2. Independent concentrated mass motions and stiff corpses of the mechanical oscillation system are those of the driver's vertical motions, the middle part of the bus (passenger 1), the passenger's rear overhang (passenger 2), the center of gravity of the bus, the mass elastic suspension system, the front and rear axle center of gravity, and the angular movement of the rear axle. Fig. 3 provides an overview of the suspension parts on the rear axle with characteristic geometry utilized to calculate the appropriate accessory model oscillation stiffness and damping shown in Fig. 2. The effects of vibration from the road on the driver's body and passengers rely on the characteristics of the seat suspension system as well. A pneumatic elastic suspension and a shock absorber are provided for the driver's seat. Passenger seat suspension is stiff, and the seat airbags are made of strong polyurethane foam. Fig. 4 depicts the position of the fully loaded bus's center of gravity. The assumptions chosen for the bus oscillatory model are as follows: the bus is consistent with the longitudinal center of the gravitational axis (x-axis). All potential concentrated mass movements around the stationary equilibrium position are modest; stiff bodies include the bus-body, the front and rear axles and the bus

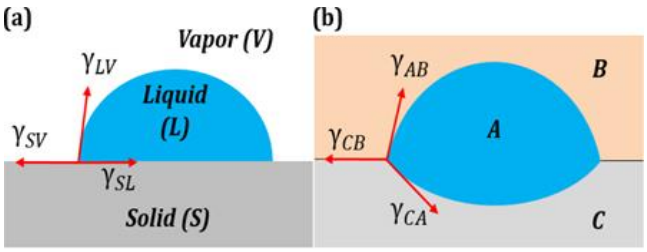

Fig. 4(a) Surface tension forces at the three-phase line on a non-deformable solid surface, (b) The equilibrium of surface tensions at the three phase line of liquid phases A, B and C

Table 1 Dimensionless natural frequency of straight double system subjected to different size scale coefficients

μ	Present	Murmu and Adhikari (2010)
0	9.8696	9.8696
0.1	9.4158	9.4158
0.2	8.3569	8.3569
0.3	7.1823	7.1823
0.4	6.1455	6.1455
0.5	5.3002	5.3002
0.6	4.6253	4.6253
0.7	4.0854	4.0854
0.8	3.6487	3.6487
0.9	3.2909	3.2909
1	2.9935	2.9935

engine is included in the bus body, so that engine oscillatory excitation is not considered; therefore, the properties of all damping and elastic elements are linear. The road surface of the bus's wheels is in continuous contact, so the bus is in continual, steady movement on a straight path. In the car's suspension system, the characteristics of the springs and shock absorbers are nonlinear as well as the properties of the tires and other elastic vehicle components. The nonlinear oscillatory model vehicle is, therefore, utilized for conducting analysis of oscillations In (Zhu and Ishitobi 2004), the nonlinear 4DOF oscillatory model was given, while (Zhu and Ishitobi 2006) the vehicle's chaotic response was examined with a nonlinear oscillatory 7DOF space oscillatory model. Table 1 additionally contain all parameter values from accessible literature (Mladenović 1997), which are employed in the simulation. The equivalent rigidity and damping values are calculated in the following terms according to Fig. 3: The following are

$$C_z = C'_2 + C''_2 = \frac{C_2(b-r_a)^2}{b^2} + \frac{C_2(b-r_a)^2}{b^2}, \quad (1)$$

$$b_z = b'_2 + b''_2 = \frac{b_2(b-r_a)^2}{b^2} + \frac{b_2(b-r_a)^2}{b^2}, \quad (2)$$

$$m_u z_u + b_{su} z_u + c_{su} z_u - b_{su} z - c_{su} z - s_1 b_{su} \varphi - s_1 c_{su} \varphi + s_2 b_{su} \theta + s_2 c_{su} \theta = 0, \quad (3)$$

$$m_{p1} z_{p1} + b_{sp1} z_{p1} + c_{sp1} z_{p1} - b_{sp1} z - c_{sp1} z - s_3 b_{sp1} \varphi - s_3 c_{sp1} \varphi + s_4 b_{sp1} \theta + s_4 c_{sp1} \theta = 0, \quad (4)$$

$$m_{p2} z_{p2} + b_{sp2} z_{p2} + c_{sp2} z_{p2} - b_{sp2} z - c_{sp2} z - s_5 b_{sp2} \varphi - s_5 c_{sp2} \varphi + s_6 b_{sp2} \theta + s_6 c_{p2} \theta = 0, \quad (5)$$

$$\begin{aligned} &\mathrm{Mz} + (b_{su} + b_{sp1} + b_{sp2} + 2b_p + 2b_z) z \\ &+ c_{su} + c_{sp1} + c_{sp2} + 2c_p + 2c_z) z \\ &+ s_1 b_{su} + s_3 b_{sp1} + s_5 b_{sp2}) \varphi \\ &+ s_1 c_{su} + s_3 c_{sp1} + s_5 c_{sp2}) \varphi \\ &- (s_2 b_{su} + s_4 b_{sp1} + s_6 b_{sp2} + 2ab_p - 2bb_z) \theta \\ &- (s_2 c_{su} + s_4 c_{sp1} - s_6 c_{p2} + 2ac_p - 2bc_z) \theta \\ &- b_{su} z_u - c_{su} z_u - b_{sp1} z_{p1} - c_{sp1} z_{p1} - b_{sp2} z_{p2} \\ &- c_{sp2} z_{p2} - 2b_p z_1 - 2c_p z_1 - 2b_z z_2 - 2c_z z_2 = 0, \end{aligned} \quad (6)$$

$$\begin{aligned} &j_x \varphi + (s_1^2 b_{su} + s_3^2 b_{sp1} + s_5^2 b_{sp2} + 2e_1^2 b_p + 2e_2^2 b_z) \varphi \\ &+ (s_1^2 c_{su} + s_3^2 c_{sp1} + s_5^2 c_{sp2} + 2e_1^2 c_p + 2e_2^2 c_z) \varphi \\ &- s_1 b_{su} z_u - s_1 c_{su} z_u + s_3 b_{sp1} z_{p1} + s_3 c_{sp1} z_{p1} \\ &- s_5 b_{sp2} z_{p2} - s_5 c_{sp2} z_{p2} + (s_1 b_{su} - s_3 b_{sp1} - s_5 b_{sp2}) z \\ &+ (s_1 c_{su} - s_3 c_{sp1} + s_5 c_{sp2}) z \\ &- (s_1 s_2 b_{su} - s_3 s_4 b_{sp1} - s_5 s_6 b_{sp2}) \theta \\ &- (s_1 s_2 c_{su} - s_3 s_4 c_{sp1} - s_5 s_6 c_{sp2}) \theta - 2e_1^2 b_p \varphi_1 \\ &- 2e_1^2 c_p \varphi_1 - 2e_2^2 b_z \varphi_2 - 2e_2^2 c_z \varphi_2 = 0, \end{aligned} \quad (7)$$

$$\begin{aligned} &j_y \theta + (s_2^2 b_{su} + s_4^2 b_{sp1} + s_6^2 b_{sp2} + 2a^2 b_p + 2b^2 b_z) \theta \\ &+ s_2^2 c_{su} + s_4^2 c_{sp1} + s_6^2 c_{sp2} + 2a^2 c_p + 2b^2 c_z) \theta \end{aligned} \quad (8)$$

$$\begin{aligned} &s_2 b_{su} z_u + s_2 c_{su} + s_4 b_{sp1} z_{p1} + s_4 c_{sp1} z_{p1} - s_6 b_{sp2} z_{p2} \\ &- s_6 c_{sp2} z_{p2} - \begin{pmatrix} s_2 b_{su} + s_4 b_{sp1} - s_6 b_{sp2} + 2ab_p \\ + 2bb_z \end{pmatrix} z \\ &- (s_2 c_{su} + s_4 c_{sp1} - s_6 c_{sp2} + 2ac_p - 2bc_z) z \\ &- (s_1 s_2 c_{su} - s_3 s_4 c_{sp1} - s_5 s_6 c_{sp2} + 2ac_p - 2bc_z) z \\ &- (s_1 s_2 b_{su} - s_3 s_4 b_{sp1} - s_5 s_6 b_{sp2}) \varphi \\ &- (s_1 s_2 c_{su} - s_3 s_4 c_{sp1} - s_5 s_6 c_{sp2}) \varphi \\ &+ 2ab_p z_1 + 2ac_p z_1 + 2bb_z z_2 + 2bc_z z_2 = 0, \end{aligned} \quad (9)$$

$$\begin{aligned} &m_{pm} z_{p1} + 2(b_p + b_{pp}) z_1 + 2(c_p + c_{pp}) z_1 \\ &- 2b_p z - 2c_p z + 2ab_p \theta + 2ac_p \theta \\ &= b_{pp\zeta pd} + c_{pp\zeta pd} + b_{pp\zeta pl} + c_{pp\zeta pl}, \end{aligned} \quad (10)$$

$$\begin{aligned} &j_{x1} \varphi_1 + 2(e_1^2 b_p + f_1^2 b_{pp}) \varphi_1 + 2(e_1^2 c_p + f_1^2 c_{pp}) \varphi_1 \\ &- 2e_1^2 b_p \varphi - 2e_1^2 c_p \varphi \\ &= f_1 b_{pp\zeta pd} - f_1 c_{pp\zeta pd} + f_1 b_{pp\zeta pl} + f_1 c_{pp\zeta pl} \end{aligned} \quad (11)$$

$$\begin{aligned} &m_{zm} z_2 + 2(b_z + b_{zp}) z_2 + 2(c_z + c_{zp}) z_2 \\ &- 2b_z z - 2c_z z - 2bb_z \theta - 2bc_z \theta \\ &= b_{zp\xi zd} + c_{zp\xi zd} + b_{zp\xi zl} + c_{zp\xi zl}, \end{aligned} \quad (12)$$

$$\begin{aligned} &j_{x2} \varphi_2 + 2(e_2^2 b_z + f_2^2 b_{zp}) \varphi_2 + 2(e_2^2 c_z + f_2^2 c_{zp}) \varphi_2 \\ &- 2e_2^2 b_z \varphi - 2e_2^2 c_z \varphi \\ &= -f_2 b_{zp\xi zd} - f_2 c_{zp\xi zd} + f_2 b_{zp\xi zl} + f_2 c_{zp\xi zl} \end{aligned} \quad (13)$$

1.2 Vibration data measurement and analysis

The study tested vibration levels in several trucks from different areas of the globe. A more detailed article was written on this topic, which deals with both transport by road and rail. The 3X90 Shock and Vibration Enterprise (SAVER) Model was designed by the company, Lansmont Corp. (Monterey, CA, USA) (Fig. 2). It is a piezo-electric three-axis accelerometer that detects shock (impact, drop), vibration, temperature and moisture conditions in transport and handling. On the back of the platform, the recorders were mounted. This place provides the highest measurement of vertical vibration.

1.3 Problem statement

The curve has unconstrained in-plane vibration, as seen in Fig. 2. The curvature of the radius and its thickness are respectively R and H. For all exterior surfaces, additional surface effects are expected. For a curved Euler Bernoulli beam, the dynamic balance equations are given as:

$$\frac{\partial v}{\partial \theta} + P = \rho AR\frac{\partial^2 u_r}{\partial t^2} + Rb\rho^s\left(\frac{\partial^2 {u_r}^+}{\partial t^2} + \frac{\partial^2 {u_r}^-}{\partial t^2}\right)$$
$$\frac{\partial P}{\partial \theta} - V = \rho AR\frac{\partial^2 u_\theta}{\partial t^2} + Rb\rho^s\left(\frac{\partial^2 {u_\theta}^+}{\partial t^2} + \frac{\partial^2 {u_\theta}^-}{\partial t^2}\right) \quad (14)$$
$$;\frac{\partial M}{\partial \theta} + RV = 0$$

$F(\theta, t)$ *= the shearing force*

$P(\theta, t)$ *is the tensile force,*

A *= the cross sectional area*

ρ *= the mass density* (15)

ρ^s *= the surface density of the Nano ring*

b *= the width of Nano ring In Eq. (1)*

$\ddot{u}_r^+ = \ddot{u}_r^+ = \ddot{u}_r^+,\ \ddot{u}_\theta^+ + \ddot{u}_\theta^- = 2\ddot{u}_\theta$

$$P - \frac{1}{R}\frac{\partial^2 M}{\partial \theta^2} = (\rho AR + 2Rb\rho^s)\frac{\partial^2 u_r}{\partial t^2};$$
$$\frac{\partial P}{\partial \theta} + \frac{1}{R}\frac{\partial M}{\partial \theta} = (\rho AR + 2Rb\rho^s)\frac{\partial^2 u_\theta}{\partial t^2} \quad (16)$$

$$\frac{1}{R}\left(\frac{\partial^2 M}{\partial \theta^2} + \frac{\partial^4 M}{\partial \theta^4}\right) + R\left(\frac{\partial P}{\partial \theta} - \frac{\partial^2 f}{\partial \theta^2}\right) = (\rho AR + 2Rb\rho^s)\left(\frac{\partial^2 u_r}{\partial t^2} - \frac{\partial^2 u_r}{\partial t^2 \partial \theta^2}\right) \quad (17)$$

$$\frac{EI}{R^3}\left(\frac{\partial^6 u_r}{\partial \theta^6} + 2\frac{\partial^4 u_r}{\partial \theta^4} + \frac{\partial^2 u_r}{\partial \theta^2}\right) = (\rho AR + 2Rb\rho^s)\left(\frac{\partial^2 u_r}{\partial t^2} - \frac{\partial^2 u_r}{\partial t^2 \partial \theta^2} - \frac{(e_0 a)^2}{R^2}\frac{\partial^2 u_r}{\partial t^2 \partial \theta^2} + \frac{(e_0 a)^2}{R^2}\frac{\partial^6 u_r}{\partial t^4 \partial \theta^2}\right) \quad (18)$$

$$u_r = \bar{u}_r(\theta)e^{i(\omega_n t + \varphi)} \quad (19)$$

$$\frac{\partial^6 \bar{u}_r}{\partial \theta^6} + 2\frac{\partial^4 \bar{u}_r}{\partial \theta^4} + \frac{\partial^2 \bar{u}_r}{\partial \theta^2} + \beta_n\left(\bar{u}_r - \frac{\partial^2 \bar{u}_r}{\partial \theta^2}\right) = 0;$$
$$\beta_n{}^2 = \frac{2\rho AR^4 + 4R^4 b\rho^s}{2EI}\omega_n^2 \quad (20)$$

$$u_r = \sin\left(\frac{n\pi}{\alpha}\theta\right)e^{i(\omega_n t)} \quad (21)$$

$$\Omega_n^2 = \frac{\frac{EI}{R^3}(\lambda_n^6 - 2\lambda_n^4 + \lambda_n^2)}{(\rho AR + 2Rb\rho^s)\left(1 + \lambda_n^2 + \frac{(e_0 a)^2}{R^2}\lambda_n^2 + \frac{(e_0 a)^2}{R^2}\lambda_n^4\right)} \quad (22)$$
$$\frac{(R\alpha)^4 \rho A}{EI}; \lambda_n = \frac{n\pi}{\alpha}$$

$$\Omega_{n0}^2 = \frac{EI(\lambda_n^6 - 2\lambda_n^4 + \lambda_n^2)}{(\rho AR^4)\left(1 + \lambda_n^2 + \frac{(e_0 a)^2}{R^2}\lambda_n^2 + \frac{(e_0 a)^2}{R^2}\lambda_n^4\right)} \quad (23)$$
$$\frac{(R\alpha)^4 \rho A}{EI}; \lambda_n = \frac{n\pi}{\alpha}$$

2. Data collection

The transport of trucks in this investigation was carried out on the country's main distribution routes. Table 2 describes the details of the truck shipping routes. The speed of the trucks observed ranged from 30-90km/h, with an average speed of 80-90km/h in good road conditions, while in poor circumstances (mostly double-highway) it was 30-40 km/h. Figure 5 shows the Effect of Ply Orientation on the Vibration Characteristics. Table 2 shows an opening angle and a non-local impact for the first 3 non-dimensional frequencies.

2.1 Data analysis

The recorded acceleration amplitudes in the random vibration were analyzed as a function of frequency to determine the power density (PO) levels. The average PD within a narrow band of frequencies of the spectrum is calculated as follows

$$PD = \frac{1}{BW}\sum_{i=1}^{n}(RMS\ G_i^2)/N \quad (24)$$

$RMS\ G_i$ *= the root mean square acceleration value measured in* g *within a bandwidth (BW) of frequencies*

N *= the number of instants sampled*

The matching PD levels are then traced against the bandwidth frequency to create the PSD plot. The PSD plot is the vibration magnitude variation in order to determine frequencies. Data from 1 to 100 Hz as displayed as the frequency range is the most responsible for damage to the package/product during shipment. Average power density spectra were calculated and displayed in a manner similar to previous research in conveying vibration measurement.

Table 2. Opening angle and nonlocality effect on first three dimensionless frequencies with surface density (Ebrahimi and Daman 2017)

	$n = 1$			$n = 2$			$n = 3$		
μ	Opening angle			Opening angle			Opening angle		
	$\pi/8$	$\pi/4$	$\pi/2$	$\pi/8$	$\pi/4$	$\pi/2$	$\pi/8$	$\pi/4$	$\pi/2$
0	8.1476	7.5865	5.5955	33.1703	32.5904	30.3461	74.8767	74.2932	71.9936
0.1	7.7730	7.2377	5.3383	28.8664	27.5954	25.6950	54.4898	54.0652	52.3917
0.2	6.8988	6.4238	4.7379	20.6544	20.5933	18.8958	35.091	34.8175	33.7398
0.3	5.9292	5.5209	4.0720	15.5453	15.2735	14.2217	24.9667	24.7721	24.0054
0.4	5.0733	4.7239	3.4842	12.2630	12.0486	11.2189	19.1978	19.0481	18.4586
0.5	4.3755	4.0742	3.0050	10.0610	9.8851	9.2044	15.5432	15.4221	14.9447
0.6	3.8184	3.5554	2.6223	8.5046	8.3559	7.7805	13.0388	12.9372	12.5368
0.7	3.3726	3.1404	2.3162	7.3540	7.2255	6.7279	11.2214	11.1339	10.7893
0.8	3.0121	2.8047	2.0687	6.4722	6.3590	5.9211	9.8446	9.7679	9.4656
0.9	2.7167	2.5296	1.8658	5.7762	5.6752	5.2844	8.7667	8.6984	8.4291
1	2.4713	2.3011	1.6972	5.2136	5.1224	4.7697	7.9003	7.8387	7.5961

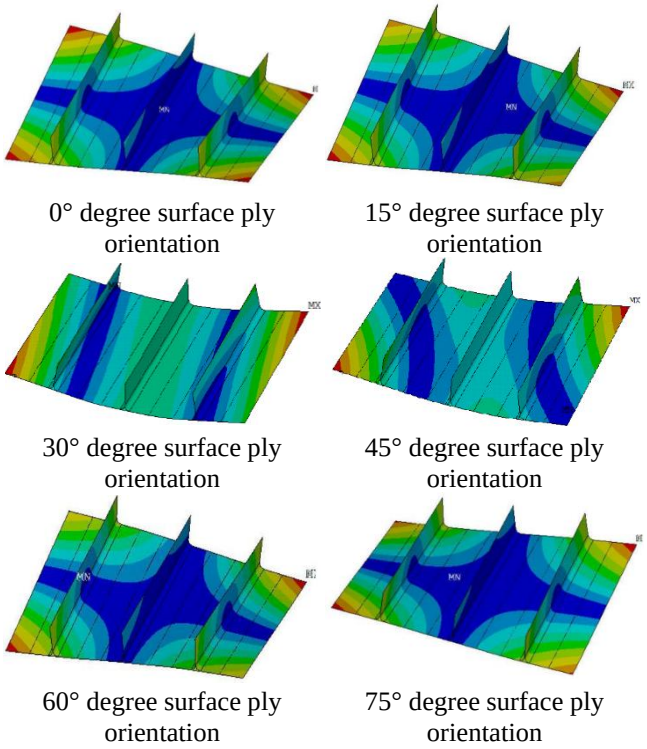

Fig. 5 The effect of ply orientation on the vibration characteristics

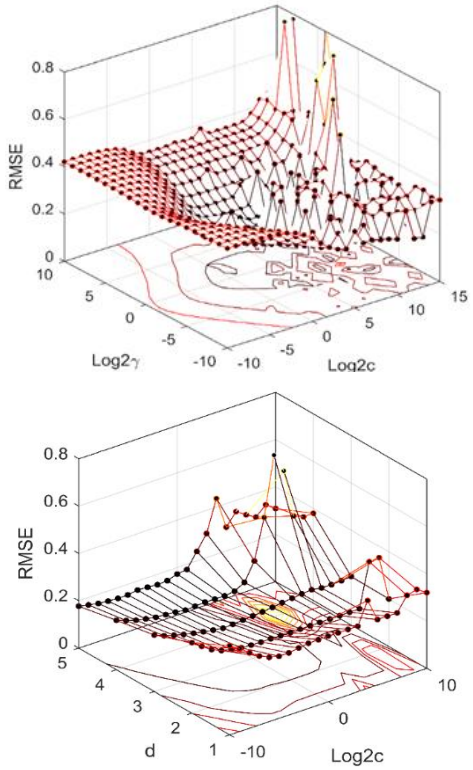

Fig. 6 3D graphical diagrams for surface effects on vibrational characteristics of public transportation

2.2 The truck vibration measurement

Fig. 6 shows the average PSD plot for transport on all axes. Data is also shown for lateral and longitudinal vibration. Because objects in their shape vary from spherical to elliptical, the damage done to every single product is the combination of vibrations and rotating effects of each fruit, together with dynamic compression in all three directions. Fig. 7 illustrates the density ranges of vibration observed by smaller city trailers used to carry products into retail shops from distribution facilities. The results of Figs. 6 and 7 demonstrate that the vertical levels of vibration observed for motorway carriers are similar to the low-frequency levels of ASTM and 1STA (1-5 Hz). However, the vertical vibration levels are significantly lower in the higher frequency range for road transport by vehicle. In the high frequency zones, the vibration levels of a smaller car from the distribution center to shops (IDe) are usually greater (Fig. 7). From the field to the packing house, the greatest vibration intensity occurred was followed by PH to DC. Between DCs in retail shops, there were the

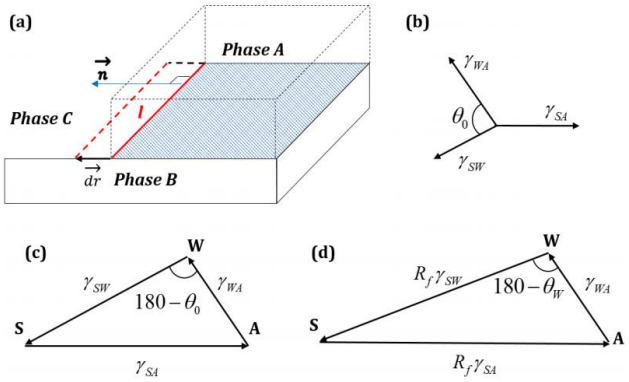

Fig. 8 (a) When the interface between A and B is displaced along the vector $\vec{dr}$, the surface tension force acts on the three-phase line l in the direction of the normal $\vec{n}$. (b) Equilibrium of surface tension vectors at the three-phase line. (c) The Neumann's triangle for a three-phase system. (d) The Neumann's triangle for a three-phase system in the Wenzel state

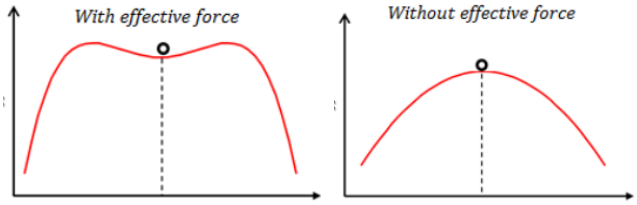

Fig. 9 (a) Unstable equilibrium corresponding to the maximum potential energy (b) A metastable equilibrium due to the stabilizing effect of the external force

lowest total vibration levels. For vertical, lateral and longitudinal orientations, the grade levels are shown in Table 2. Fig. 9 indicates (a) the instability of the balance corresponding to the maximal energy potential, (b) a metastable balance due to the external force's stabilizing impact.

3. Analysis of simulation results

Vibration impacts were evaluated in accordance with the international standard ISO 2631-1 (1997) (2631 1997) for the safety and comfort of bus riders (Fig. 8). It recommends the overall vibration value of weighted-wheel-average square-acceleration as a reference to evaluate comfortable vibration effects. This study investigates the comfort of weighted acceleration on the sites of drivers and passengers in relation to the computed root-mean square for the vertical direction.

$$Z_{rms,w} = \sqrt{\frac{1}{T}\int_0^T z_w^2\,(t)dt} \qquad (25)$$

3.1 Analysis of seat oscillatory parameters effects on driver comfort

Vibrations from the bus floor are conveyed to the driver's body through the driver's seat suspension system. Air spring (pneumatic balloon) and a hydraulic shock absorber are the main components of your driver sit suspension system. The effects of vibration on the comfort of the bus driver rely on spring rigidity and damping of the shock absorber. It is evident that the value of the driver vertical acceleration increases also when the steepness of the spring increases with a single fixed amount of the shock absorber damping. Fig. 10 illustrates the vertical acceleration signal resulting from measurements made in a previous study on the driver's site of an intercity bus, IK-302. On the "Aerodrome – Ikarbus" stretch with an asphalt-concrete road in good condition, the signal was recorded at a constant speed of bus mobility at 100 km/h. A three-axis B & K, B & K 4321 type, was used for signal recording, and a B & K type amplifier was used to boost the accelerator output. Amplifier was chosen to correspond to a 1 V voltage and a 10 m/s2 acceleration. Fig. 7 illustrates the parallel representation of experimental data (black line) and simulations of vertical acceleration signals in the driver's seat (red line). The vertical acceleration observed is 1:5 meter = s2 and 1:2 meter = s2, with virtually all values in the range of 0:6 meters = s2, 0:6 meters = s2. The maximum values of the vertical acceleration of the driver obtained using simulation for the actual oscillatory parameters for the driver seat are: 1:3 m = s2 and 1:4 m = s2 (csv 1⁄4 10; 000 N = m; bsv 1⁄4 750 Ns = m). The driver's values for a longer period of time are 0.5 m = s2, 0:5 m = s2 for a comparable change in nature as a genuine acceleration signal for a greater proportion of the simulation duration. For vertical acceleration drives determined by measurements and simulations, Table 2 displays statistical results. The mean acceleration value of the measured driver is zero, while the mean acceleration value set by simulation is zero and 0:0006 m = s2. There are also somewhat different acceleration dispersions (0:40 for measurements and 0:2228 for simulation). Therefore, the oscillatory model of the bus provides a good evaluation of the vertical acceleration sign of the driver. It must be noted that the driver's vertical acceleration signal values can be lowered with springs with a low steepness based on the findings of the simulation. Indeed, the highest values for the vertical acceleration of the driver are m = s2 for a spring rigidity of 5000 N=m and the amplitude of the shock absorber of 750 Ns=m. With 5000 N/m steepness and a 750 Ns/m damping coefficient, the lower root mean square of the weighted acceleration is 0:17 m = s2. For the spring stiffness of 15,000 N/m and a shock absorber damping coefficient of 400 Ns/m, the maximum mean raw square of the weighted driver's acceleration is 0:31 m = s2. Fig. 9 illustrates the dependency of the root mean square on the vertical acceleration of the weighted driver as a function of spring rigidity and the damping coefficient of shock-absorbing. It is apparent that lower-root medium squares are given by chairs with reduced spring rigidity. With increasing spring rigidity and lower shock-absorber damping values, the root meaning of the weighted driver's acceleration square increases. In Fig. 10, the minimum and maximum root mean squares of the weighted driver's acceleration as well as the root mean square of the weighted acceleration for driver's seat real oscillatory parameters are seen.

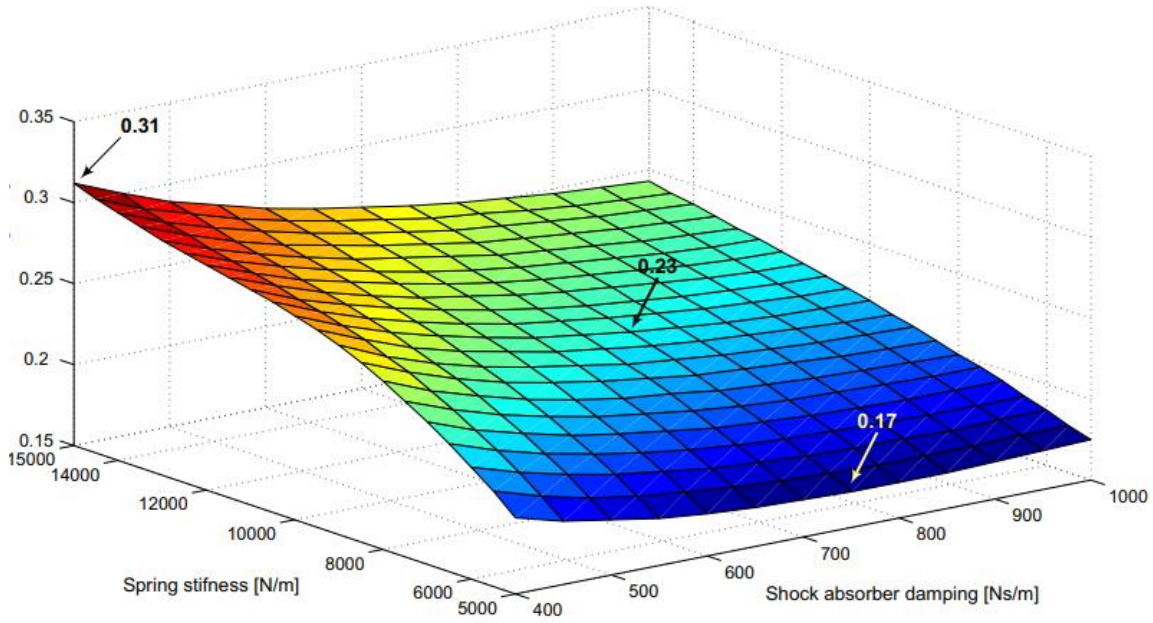

Fig. 10 Root mean square of the weighted driver's vertical acceleration as a function of the spring stiffness and shock-absorber damping coefficients of driver's seat

4. Conclusions

The intercity bus IK-301 features a spatial oscillatory model outlined in the article. The model was utilized to assess drivers and passengers' oscillatory comforts on their bus places. The root is the weighted driver's acceleration square for 100 km = h and the excitation of asphalt concrete in very good condition, passengers in the center portion, 0:23 m = s2, 0:30 m = s2, 0:62 m = s2, respectively, and the rear overhang is 0:23 m. The standard of 1997 ISO 2631-1 provides for vibrational impacts on passenger comfort in the overhang rear of the bus based on the weighing criteria. The intercity bus IK-301 features a spatial oscillatory model outlined in the article. The model was utilized to assess drivers and passengers' oscillatory comforts on their bus places. For 100 km = h and the excitation of asphalt-concrete in very excellent condition, the root is the weighted driver's acceleration square, passengers in the center portion, 0:23 m = s2, 0:30 m = s2, 0:62 m = s2, respectively, and the rear overhang is 0:23 m. The oscillatory comfort of the bus's back hang and driver is dependent on spring stiffness and the damping of the shock absorbent on the driver's seat suspension system vibrations for passenger comfort according to weighing criteria in 1997 ISO 2631-1. The results of the simulation show that with the spring steadiness of 5000 N = m and the shock absorber damping of 750 Ns = m, the lowest root mean accelerating square of 0:17 m = s2 is given by the seat. For the seat with the greatest spring stiffness of 15, 000 N = m and the lowest damping shock absorber of 400 Ns = m, the highest mean root square with a weighted acceleration of 0:31 m = s2 was obtained. This median root square value in the public transportation sector is around the comfort limit of 0:315 m = s2 following the ISO 2631-1 standard from 1997.

Acknowledgments

This project was supported by the Deanship of Scientific Research at Prince Sattam Bin Abdulaziz University under the research project No. 2020/01/17088.

References

Afsar Dizaj, E., Fanaie, N. and Zarifpour, A. (2018), "Probabilistic seismic demand assessment of steel frames braced with reduced yielding segment buckling restrained braces", *Adv. Struct. Eng.* **21**(7), 1002-1020. https://doi.org/10.1177/1369433217737115.

Afshar, A., Jahandari, S., Rasekh, H., Shariati, M., Afshar, A. and Shokrgozar, A. (2020), "Corrosion resistance evaluation of rebars with various primers and coatings in concrete modified with different additives", *Constr. Build. Mater.*, **262**, 120034. https://doi.org/10.1016/j.conbuildmat.2020.120034.

Al-Furjan, M., Habibi, M., Shan, L. and Tounsi, A. (2021), "On the vibrations of the imperfect sandwich higher-order disk with a lactic core using generalize differential quadrature method", *Compos. Struct.*, **257**, 113150. https://doi.org/10.1016/j.compstruct.2020.113150.

Alperovitch Najenson, D., Santo, Y., Masharawi, Y., Katz-Leurer, M., Ushvaev, D. and Kalichman, L. (2010), "Low back pain among professional bus drivers: ergonomic and occupational-psychosocial risk factors", *Israel Med. Assoc. J.*, **12**(1), 26. https://doi.org/10.1155/2019/6793090. eCollection 2019.

Arabnejad Khanouki, M.M., Ramli Sulong, N.H. and Shariati, M. (2010), "Investigation of seismic behaviour of *Compos. Struct.*, with concrete filled square steel tubular (CFSST) column by push-over and time-history analyses", *Proceedings of the 4th International Conference on Steel & Composite Structure*, Sydney, Australia, July.

Arabnejad Khanouki, M.M., Ramli Sulong, N.H., Shariati, M. and Tahir, M.M. (2016), "Investigation of through beam connection to concrete filled circular steel tube (CFCST) column", *J. Const. Steel Res.*, **121**, 144-162. https://doi.org/10.1016/j.jcsr.2016.01.002.

Asadolahi, S.M. and Fanaie, N. (2020), "Performance of self-centering steel moment frame considering stress relaxation in prestressed cables", *Adv. Struct. Eng.*, **23**(9), 1813-1822. https://doi.org/10.1177/1369433219900940.

Borowiec, M., Sen, A.K., Litak, G., Hunicz, J., Koszałka, G. and Niewczas, A. (2010), "Vibrations of a vehicle excited by real road profiles", *Forschung im Ingenieurwesen*, **74**(2), 99-109. https://doi.org/10.1007/s10010-010-0119-y.

Chen, C., Wang, X., Wang, Y., Yang, D., Yao, F., Zhang, W., Wang, B., Sewvandi, G. A., Yang, D. and Hu, D. (2020), "Additive manufacturing of piezoelectric materials", *Adv. Funct. Mater.*, **30**(52), 2005141, https://doi.org/10.1002/adfm.202005141.

Daie, M., Jalali, A., Suhatril, M., Shariati, M., Arabnejad Khanouki, M.M., Shariati, A. and Kazemi-Arbat, P. (2011), "A new finite element investigation on pre-bent steel strips as damper for vibration control", *Int. J. Phys. Sci.*, **6**(36), 8044-8050. https://doi.org/10.5897/ijps11.1585.

Davoodnabi, S.M., Mirhosseini, S.M. and Shariati, M. (2019), "Behavior of steel-concrete composite beam using angle shear connectors at fire condition", *Steel Compos. Struct.*, **30**(2), 141-147. https://doi.org/10.12989/scs.2019.30.2.141.

Dong, H., Zhao, B. and Deng, Y. (2018), "Instability phenomenon associated with two typical high speed railway vehicles", *Int. J. Nonlinear Mech.*, **105**, 130-145. https://doi.org/10.1016/J.IJNONLINMEC.2018.06.006.

Ebrahimi, F. and Daman, M. (2017), "Analytical investigation of the surface effects on nonlocal vibration behavior of nanosize curved beams", *Adv. Nano Res.*, **5**(1), 35-47. https://doi.org/10.12989/anr.2017.5.1.035.

Ebrahimi, F., Habibi, M. and Safarpour, H. (2019), "On modeling of wave propagation in a thermally affected GNP-reinforced imperfect nanocomposite shell", *Eng. Comput.*, **35**(4), 1375-1389. https://doi.org/10.1007/s00366-018-0669-4.

Ebrahimi, F., Hashemabadi, D., Habibi, M. and Safarpour, H. (2020), "Thermal buckling and forced vibration characteristics of a porous GNP reinforced nanocomposite cylindrical shell", *Microsyst. Technol.*, **26**(2), 461-473. https://doi.org/10.1007/s00542-019-04542-9.

Fanaie, N., Aghajani, S. and Shamloo, S. (2012), "Theoretical assessment of wire rope bracing system with soft central cylinder", *Proceedings of the 15th world conference on earthquake engineering*, Lisbon, Portugal, September.

Fanaie, N. and Shamlou, S.O. (2015), "Response modification factor of mixed structures", *Steel Compos. Struct.*, **19**(6), 1449-1466. https://doi.org/10.12989/scs.2015.19.6.1449.

Fanaie, N., Kazerani, S. and Soroushnia, S. (2017a), "Numerical study of slotted web drilled flange moment frame connection", *Int. J. Numer. Method Civil Eng.*, **1**(3), 16-23. https://doi.org/10.1016/j.jcsr.2011.06.003.

Fanaie, N. and Tahriri, M. (2017b), "Stability and stiffness analysis of a steel frame with an oblique beam using method of least work", *J. Const. Steel Res.*, 137, 342-357 DOI: https://doi.org/10.1016/j.jcsr.2017.06.032.

Fanaie, N., Faegh, S. S. and Partovi, F. (2019), "An improved and innovative formulation for calculating amplified elastic story drift induced by RBS connections in steel moment frames", *J. Const. Steel Res.*, 160, 510-527. https://doi.org/10.1016/j.jcsr.2019.06.003.

Ghabussi, A., Ashrafi, N., Shavalipour, A., Hosseinpour, A., Habibi, M., Moayedi, H., Babaei, B. and Safarpour, H. (2019), "Free vibration analysis of an electro-elastic GPLRC cylindrical shell surrounded by viscoelastic foundation using modified length-couple stress parameter", *Mech. Based Des. Struct.*, 1-25. https://doi.org/10.1080/15397734.2019.1705166.

Ghanbari Ghazijahani, T., Nabati, A., Azandariani, M.G. and Fanaie, N. (2020), "Crushing of steel tubes with different infills under partial axial loading", *Thin Wall. Struct.*, **149**, 106614. https://doi.org/10.1016/j.tws.2020.106614.

Goudarzi, A., Ghassemieh, M., Fanaie, N., Laefer, D. F. and Baei, M. (2016), "Axial load effects on flush end-plate moment connections", *Proceedings of the Institution of Civil Engineers Structures and Buildings*, **170**(3), 199-210. https://doi.org/10.1016/S0141-0296(97)00050-3.

Habibi, M., Hashemabadi, D. and Safarpour, H. (2019), "Vibration analysis of a high-speed rotating GPLRC nanostructure coupled with a piezoelectric actuator", *Eur. Phys. J. Plus.*, **134**(6), 1-23 https://doi.org/10.1140/epjp/i2019-12742-7.

Habibi, M., Safarpour, M. and Safarpour, H. (2020), "Vibrational characteristics of a FG-GPLRC viscoelastic thick annular plate using fourth-order Runge-Kutta and GDQ methods", *Mech. Based Des. Struct.*, 1-22. https://doi.org/10.1080/15397734.2020.1779086.

Hajilak, Z.E., Pourghader, J., Hashemabadi, D., Bagh, F.S., Habibi, M. and Safarpour, H. (2019), "Multilayer GPLRC composite cylindrical nanoshell using modified strain gradient theory", *Mech. Based Des. Struct.* https://doi.org/10.1080/15397734.2019.1566743.

Hamidian, M., Shariati, M., Arabnejad, M. and Sinaei, H. (2011), "Assessment of high strength and light weight aggregate concrete properties using ultrasonic pulse velocity technique", *Int. J. Phys. Sci.*, **6**(22), 5261-5266 https://doi.org/10.5897/IJPS11.1081.

Heydari, A. and Shariati, M. (2018), "Buckling analysis of tapered BDFGM nano-beam under variable axial compression resting on elastic medium", *Struct. Eng. Mech.*, **66**(6), 737-748. https://doi.org/10.12989/sem.2018.66.6.737.

Hong, XC., Wang, G.Y., Liu, J., Song, L. and Wu, E.T. (2021), "Modeling the impact of soundscape drivers on perceived birdsongs in urban forests", *J. Clean. Prod.*, **292**, 125315. https://doi.org/10.1016/j.jclepro.2020.125315.

Hosseinpour, E., Baharom, S., Badaruzzaman, W.H.W., Shariati, M. and Jalali, A. (2018), "Direct shear behavior of concrete filled hollow steel tube shear connector for slim-floor steel beams", *Steel Compos. Struct.*, **26**(4), 485-499. https://doi.org/10.12989/scs.2018.26.4.485.

Hou, Z., Lu, H., Li, Y., Yang, L. and Gao, Y. (2021), "Direct ink writing of materials for electronics-related applications: A mini review", *Front. Mater.*, **8**, 91. https://doi.org/10.3389/fmats.2021.647229.

Hu, J., Zhang, H., Li, Z., Zhao, C., Xu, Z. and Pan, Q. (2020), "Object traversing by monocular UAV in outdoor environment", *Asian J. Control*. https://doi.org/10.1002/asjc.2415.

Huang, X., Zhang, Y., Moradi, Z. and Shafiei, N. (2021a), "Computer simulation via a couple of homotopy perturbation methods and the generalized differential quadrature method for nonlinear vibration of functionally graded non-uniform micro-tube", *Eng. Comput.*, 1-18. https://doi.org/10.1007/s00366-021-01395-7.

Huang, X., Zhu, Y., Vafaei, P., Moradi, Z. and Davoudi, M. (2021b), "An iterative simulation algorithm for large oscillation of the applicable 2D-electrical system on a complex nonlinear substrate", *Eng. Comput.*, 1-13. https://doi.org/10.1007/S00366-021-01320-Y.

Ismail, M., Shariati, M., Abdul Awal, A.S.M., Chiong, C.E., Sadeghipour Chahnasir, E., Porbar, A., Heydari, A. and Khorami, M. (2018), "Strengthening of bolted shear joints in industrialized ferrocement construction", *Steel Compos. Struct.*, **28**(6), 681-690 DOI: https://doi.org/10.12989/scs.2018.28.6.681.

Jalali, A., Daie, M., Nazhadan, S.V.M., Kazemi-Arbat, P. and Shariati, M. (2012), "Seismic performance of structures with pre-bent strips as a damper", *Int. J. Phys. Sci.*, **7**(26), 4061-4072. https://doi.org/10.1002/eqe.880.

Ji, X., Hou, C., Gao, Y., Xue, Y., Yan, Y. and Guo, X. (2020a),

"Metagenomic analysis of gut microbiota modulatory effects of jujube (Ziziphus jujuba Mill.) polysaccharides in a colorectal cancer mouse model", *Food Function*. **11**(1), 163-173. https://doi.org/10.1039/C9FO02171J.

Ji, X., Hou, C., Shi, M., Yan, Y. and Liu, Y. (2020b), "An Insight into the research concerning Panax ginseng CA Meyer polysaccharides: A review", *Food Rev. Int.*, 1-17. https://doi.org/10.1080/87559129.2020.1771363.

Jiao, J., Ghoreishi, S.M., Moradi, Z. and Oslub, K. (2021), "Coupled particle swarm optimization method with genetic algorithm for the static–dynamic performance of the magneto-electro-elastic nanosystem", *Eng. Comput.*, 1-15. https://doi.org/10.1007/s00366-021-01391-x.

Katebi, J., Shoaei-parchin, M., Shariati, M., Trung, N.T. and Khorami, M. (2019), "Developed comparative analysis of metaheuristic optimization algorithms for optimal active control of structures", *Eng. Comput.*, 1-20. https://doi.org/10.1007/s00366-019-00780-7.

Kazerani, S., Fanaie, N. and Soroushnia, S. (2014), "Seismic behavior of drilled beam section in moment connections", *Num. Methods Civil Eng.*, **1**(2), 21-28. https://doi.org/10.1016/j.jcsr.2006.06.030.

Khorami, M., Alvansazyazdi, M., Shariati, M., Zandi, Y., Jalali, A. and Tahir, M. (2017), "Seismic performance evaluation of buckling restrained braced frames (BRBF) using incremental nonlinear dynamic analysis method (IDA)", *Proceedings of the 9th fib International PhD Symposium in Civil Engineering: Karlsruhe Institute of Technology (KIT)*, Karlsruhe, Germany, July. http://doi.org/10.12989/eas.2017.13.6.531.

Khorramian, K., Maleki, S., Shariati, M., Jalali, A. and Tahir, M. (2017), "Numerical analysis of tilted angle shear connectors in steel-concrete composite systems", *Steel Compos. Struct.*, **23**(1), 67-85. https://doi.org/10.12989/scs.2017.23.1.067.

Khorramian, K., Maleki, S., Shariati, M. and Ramli Sulong, N.H. (2016), "Behavior of tilted angle shear connectors", *Plos One*, **11**(2). https://doi.org/10.1371/journal.pone.0144288.

Kompier, M.A. (1996), Bus drivers: Occupational stress and stress prevention, International Labour Office Geneva.

Li, D., Toghroli, A., Shariati, M., Sajedi, F., Bui, D.T., Kianmehr, P., Mohamad, E.T. and Khorami, M. (2019), "Application of polymer, silica-fume and crushed rubber in the production of Pervious concrete", *Smart Struct. Syst.*, **23**(2), 207-214. https://doi.org/10.12989/sss.2019.23.2.207.

Litak, G., Borowiec, M., Hunicz, J., Koszałka, G. and Niewczas, A. (2009), "Vibrations of a delivery car excited by railway track crossing", *Chaos Soliton Fract.*, **42**(1), 270-276. https://doi.org/10.1016/j.chaos.2008.11.020.

Luo, Z., Sinaei, H., Ibrahim, Z., Shariati, M., Jumaat, Z., Wakil, K., Pham, B.T., Mohamad, E.T. and Khorami, M. (2019), "Computational and experimental analysis of beam to column joints reinforced with CFRP plates", *Steel Compos. Struct.*, **30**(3), 271-280. http://doi.org/10.12989/scs.2019.30.3.271.

Ma, H. J., Xu, L. X. and Yang, G.H. (2021a), "Multiple environment integral reinforcement learning-based fault-tolerant control for affine nonlinear systems", *IEEE T. Cybernet.*, **51**. https://doi.org/10.1109/TCYB.2018.2889679.

Ma, L., Liu, X. and Moradi, Z. (2021b), "On the chaotic behavior of graphene-reinforced annular systems under harmonic excitation", *Eng. Comput.*, 1-25. https://doi.org/10.1007/s00366-020-01210-9.

Mansouri, I., Shariati, M., Safa, M., Ibrahim, Z., Tahir, M. and Petković, D. (2019), "Analysis of influential factors for predicting the shear strength of a V-shaped angle shear connector in composite beams using an adaptive neuro-fuzzy technique", *J. Intell. Manuf.*, **30**(3), 1247-1257. https://doi.org/10.1007/s10845-017-1306-6.

Mehrabi, P., Shariati, M., Kabirifar, K., Jarrah, M., Rasekh, H., Trung, N.T., Shariati, A. and Jahandari, S. (2021), "Effect of pumice powder and nano-clay on the strength and permeability of fiber-reinforced pervious concrete incorporating recycled concrete aggregate", *Constr. Build. Mater.*, **287**, 122652. https://doi.org/10.1016/j.conbuildmat.2021.122652.

Milovancevic, M., Marinović, J. S., Nikolić, J., Kitić, A., Shariati, M., Trung, N.T., Wakil, K. and Khorami, M. (2019), "UML diagrams for dynamical monitoring of rail vehicles", *Physica A.*, 121169. https://doi.org/10.1016/j.physa.2019.121169.

Mladenović, D. (1997), "An analysis of constructions parameters impact on the oscillatory behaviour of the bus", M.Sc. Dissertation, The Faculty of Transport and Traffic Engineering, Belgrade, Serbia.

Moghadam, H., Fanaei, N. and Motazedian, D. (2010), "Estimation of stress drop for some large shallow earthquakes using stochastic point source and finite fault modeling", Scientia Iranica, **17**(3). https://doi.org/10.1093/gji/ggw374.

Mohammadhassani, M., Nezamabadi Pour, H., Suhatril, M. and Shariati, M. (2013), "Identification of a suitable ANN architecture in predicting strain in tie section of concrete deep beams", *Struct. Eng. Mech.*, **46**(6), 853-868. http://doi.org/10.12989/sem.2013.46.6.853.

Mohammadhassani, M., Akib, S., Shariati, M., Suhatril, M. and Arabnejad Khanouki, M.M. (2014a), "An experimental study on the failure modes of high strength concrete beams with particular references to variation of the tensile reinforcement ratio", *Eng. Fail. Anal.*, **41**, 73-80. https://doi.org/10.1016/j.engfailanal.2013.08.014.

Mohammadhassani, M., Nezamabadi-Pour, H., Suhatril, M. and Shariati, M. (2014b), "An evolutionary fuzzy modelling approach and comparison of different methods for shear strength prediction of high-strength concrete beams without stirrups", *Smart Struct. Syst.*, **14**(5), 785-809. https://doi.org/10.12989/sss.2014.14.5.785.

Mohammadhassani, M., Suhatril, M., Shariati, M. and Ghanbari, F. (2014c), "Ductility and strength assessment of HSC beams with varying of tensile reinforcement ratios", *Struct. Eng. Mech.*, **48**(6), 833-848. https://doi.org/10.12989/sem.2013.48.6.833.

Naghipour, M., Niak, K.M., Shariati, M. and Toghroli, A. (2020a), "Effect of progressive shear punch of a foundation on a reinforced concrete building behavior", *Steel Compos. Struct.*, **35**(2), 279-294. https://doi.org/10.12989/scs.2020.35.2.279.

Naghipour, M., Yousofizinsaz, G. and Shariati, M. (2020b), "Experimental study on axial compressive behavior of welded built-up CFT stub columns made by cold-formed sections with different welding lines", *Steel Compos. Struct.*, **34**(3), 347. https://doi.org/10.12989/scs.2020.34.3.347.

Najarkolaie, K.F., Mohammadi, M. and Fanaie, N. (2017), "Realistic behavior of infilled steel frames in seismic events: experimental and analytical study", *Bull. Earthq. Eng.* **15**(12), 5365-5392. https://doi.org/10.1007/s10518-017-0173-z.

Nasrollahi, S., Maleki, S., Shariati, M., Marto, A. and Khorami, M. (2018), "Investigation of pipe shear connectors using push out test", *Steel Compos. Struct.*, **27**(5), 537-543. http://doi.org/10.12989/scs.2018.27.5.537.

Nelson, C.M. and Brereton, P.F. (2005), "The European vibration directive", *Ind. Health*, **43**(3), 472-479. https://doi.org/10.2486/indhealth.43.472.

Ni, Z., Cao, X., Wang, X., Zhou, S., Zhang, C., Xu, B. and Ni, Y. (2021), "Facile synthesis of copper (I) oxide nanochains and the photo-thermal conversion performance of its nanofluids", *Coatings*, **11**(7), 749. https://doi.org/10.3390/coatings11070749.

Nosrati, A., Zandi, Y., Shariati, M., Khademi, K., Darvishnezhad Aliabad, M., Marto, A., Mu'azu, M., Ghanbari, E., Mandizadeh, M.B. and Shariati, A. (2018), "Portland cement structure and its

major oxides and fineness", *Smart Struct. Syst.*, **22**(4), 425-432. https://doi.org/10.12989/sss.2018.22.4.425.

Okunribido, O.O., Shimbles, S. J., Magnusson, M. and Pope, M. (2007), "City bus driving and low back pain: a study of the exposures to posture demands, manual materials handling and whole-body vibration", *Appl. Ergon.*, **38**(1), 29-38. https://doi.org/10.1016/j.apergo.2006.01.006.

Paknahad, M., Shariati, M., Sedghi, Y., Bazzaz, M. and Khorami, M. (2018), "Shear capacity equation for channel shear connectors in steel-concrete composite beams", *Steel Compos. Struct.*, **28**(4), 483-494. https://doi.org/10.12989/scs.2018.28.4.483.

Partovi, F. and Fanaie, N. (2020), "Controlling deflection of long steel I-shaped girder bridge using two V-shaped pre-tensioning cables", *J. Cent. South Univ. T.*, **27**(2), 566-577. https://doi.org/10.1007/s11771-020-4317-y.

Pečeliūnas, R., Lukoševičienė, O. and Prentkovskis, O. (2003), "A mathematical model of the vibrating system equivalent to the vehicle in the mode of emergency braking", *Transport*, **18**(3), 136-142. https://doi.org/10.1080/16483840.2003.10414082.

Pečeliūnas, R., Prentkovskis, O., Garbinčius, G., Nagurnas, S. and Pukalskas, S. (2005), "Experimental research into motor vehicle oscillations in the case of changeable deceleration", *Transport*, **20**(5), 171-175. https://doi.org/10.1080/16484142.2005.9638016.

Picu, A. (2009), "Whole body vibration analysis for bus drivers", *SISoM*. https://doi.org/10.1016/j.ergon.2012.10.003.

Pourjabari, A., Hajilak, Z.E., Mohammadi, A., Habibi, M. and Safarpour, H. (2019), "Effect of porosity on free and forced vibration characteristics of the GPL reinforcement composite nanostructures", *Comput. Math. Appl.*, **77**(10), 2608-2626. https://doi.org/10.1016/j.

Qi, C. and Fourie, A. (2019), "Cemented paste backfill for mineral tailings management: Review and future perspectives", *Miner. Eng.*, **144**, 106025. https://doi.org/10.1016/j.mineng.2019.106025.

Qi, C., Spagnoli, D. and Fourie, A. (2020), "DFT-D study of single water adsorption on low-index surfaces of calcium silicate phases in cement", *Appl. Surf. Sci.*, **518**, 146255. https://doi.org/10.1016/j.apsusc.2020.146255.

Qiao, Y.X., Sheng, S.L., Zhang, L.M., Chen, J., Yang, L.L., Zhou, H.L., Wang, Y.X., Li, H.B. and Zheng, Z.B. (2021), "Friction and wear behaviors of a high nitrogen austenitic stainless steel Fe-19Cr-15Mn-0.66 N", *J. Min. Metall., Section B*, 25-25. https://doi.org/10.2298/JMMB201026025Q.

Rajaei, S., Shoaei, P., Shariati, M., Ameri, F., Musaeei, H.R., Behforouz, B. and de Brito, J. (2021), "Rubberized alkali-activated slag mortar reinforced with polypropylene fibres for application in lightweight thermal insulating materials", *Constr. Build. Mater.*, **270**, 121430. https://doi.org/10.1016/j.conbuildmat.2020.121430.

Razavian, L., Naghipour, M., Shariati, M. and Safa, M. (2020), "Experimental study of the behavior of composite timber columns confined with hollow rectangular steel sections under compression", *Struct. Eng. Mech.*, **74**(1), 145-156. https://doi.org/10.12989/sem.2020.74.1.145.

Rezaeian, A., Jahanbakhti, E. and Fanaie, N. (2020), "Numerical study of panel zone in a moment connection without continuity plates", *J. Earthq. Eng.*, 1-19. http://doi.org/10.1080/13632469.2019.1695021.

Sadeghipour Chahnasir, E., Zandi, Y., Shariati, M., Dehghani, E., Toghroli, A., Mohamed, E.T., Shariati, A., Safa, M., Wakil, K. and Khorami, M. (2018), "Application of support vector machine with firefly algorithm for investigation of the factors affecting the shear strength of angle shear connectors", *Smart Struct. Syst.*, **22**(4), 413-424. http://doi.org/10.12989/sss.2018.22.4.413.

Safa, M., Shariati, M., Ibrahim, Z., Toghroli, A., Baharom, S.B., Nor, N.M. and Petkovic, D. (2016), "Potential of adaptive neuro fuzzy inference system for evaluating the factors affecting steel-concrete composite beam's shear strength", *Steel Compos. Struct.*, **21**(3), 679-688. https://doi.org/10.12989/scs.2016.21.3.679.

Safa, M., Maleka, A., Arjomand, M.A., Khorami, M. and Shariati, M. (2019), "Strain rate effects on soil-geosynthetic interaction in fine-grained soil", *Geomech. Eng.*, **19**(6), 533-542. https://doi.org/10.5539/jsd.v10n2p238.

Safa, M., Sari, P.A., Shariati, M., Suhatril, M., Trung, N.T., Wakil, K. and Khorami, M. (2020), "Development of neuro-fuzzy and neuro-bee predictive models for prediction of the safety factor of eco-protection slopes", *Physica A.* 124046. https://doi.org/10.1016/j.physa.2019.124046.

Safarpour, H., Hajilak, Z.E. and Habibi, M. (2019), "A size-dependent exact theory for thermal buckling, free and forced vibration analysis of temperature dependent FG multilayer GPLRC composite nanostructures restring on elastic foundation", *Int. J. Mech. Mater. Des.*, **15**(3), 569-583. http://doi.org/10.1007/s10999-018-9431-8.

Sajedi, F. and Shariati, M. (2019), "Behavior study of NC and HSC RCCs confined by GRP casing and CFRP wrapping", *Steel Compos. Struct.*, **30**(5), 417-432. https://doi.org/10.12989/scs.2019.30.5.417.

Sedghi, Y., Zandi, Y., Shariati, M., Ahmadi, E., Moghimi Azar, V., Toghroli, A., Safa, M., Tonnizam Mohamad, E., Khorami, M. and Wakil, K. (2018), "Application of ANFIS technique on performance of C and L shaped angle shear connectors", *Smart Struct. Syst.*, **22**(3), 335-340. https://doi.org/10.12989/sss.2018.22.3.335.

Shah, S., Ramli Sulong, N.H., Shariati, M., Khan, R. and Jumaat, M. (2016a), "Behavior of steel pallet rack beam-to-column connections at elevated temperatures", *Thin Wall. Struct.*, **106**, 471-483. https://doi.org/10.1016/j.tws.2016.05.021.

Shah, S., Sulong, N.R., Jumaat, M. and Shariati, M. (2016b), "State-of-the-art review on the design and performance of steel pallet rack connections", *Eng. Fail. Anal.*, **66**, 240-258. https://doi.org/10.1016/j.engfailanal.2016.04.017.

Shah, S., Sulong, N.R., Khan, R., Jumaat, M. and Shariati, M. (2016c), "Behavior of industrial steel rack connections", *Mech. Syst. Signal Pr.*, **70**, 725-740. http://doi.org/10.1016/j.ymssp.2015.08.026.

Shah, S., Sulong, N.R., Shariati, M. and Jumaat, M. (2015), "Steel rack connections: Identification of most influential factors and a comparison of stiffness design methods", *Plos One*, **10**(10), e0139422. http://doi.org/10.1371/journal.pone.0139422.

Shahabi, S., Ramli Sulong, N.H., Shariati, M. and Shah, S. (2016), "Performance of shear connectors at elevated temperatures-A review", *Steel Compos. Struct.*, **20**(1), 185-203. https://doi.org/10.12989/scs.2016.20.1.185.

Shao, H.M., Shen, X.Y., Li, X.T., Cui, Y., Zhang, W., Shao, Z.C. and Zhai, Y.C. (2021), "Growth mechanism and photocatalytic evaluation of flower-like ZnO micro-structures prepared with SDBS assistance", *Int. J. Miner. Metall. Mater.*, **28**(4), 729-737. https://doi.org/10.1007/s10854-015-4051-7.

Shariati, A., Mohammad-Sedighi, H., Żur, K.K., Habibi, M. and Safa, M. (2020), "On the vibrations and stability of moving viscoelastic axially functionally graded nanobeams", *Materials*, **13**(7), 1707. https://doi.org/10.3390/ma13071707.

Sinaei, H., Jumaat, M.Z. and Shariati, M. (2011), "Numerical investigation on exterior reinforced concrete Beam-Column joint strengthened by composite fiber reinforced polymer (CFRP)", *Int. J. Phys. Sci.*, **6**(28), 6572-6579. https://doi.org/10.5897/IJPS11.1225

Sinaei, H., Shariati, M., Abna, A.H., Aghaei, M. and Shariati, A. (2012), "Evaluation of reinforced concrete beam behaviour

using finite element analysis by ABAQUS", *Sci. Res. Essay*, **7**(21), 2002-2009. https://doi.org/10.5897/SRE11.1393.

Suhatril, M., Osman, N., Sari, P.A., Shariati, M. and Marto, A. (2019), "Significance of surface eco-protection techniques for cohesive soils slope in Selangor, Malaysia", *Geotech. Geologic. Eng.*, **37**(3), 2007-2014. https://doi.org/10.1007/s10706-018-0740-3(0123.

Tahmasbi, F., Maleki, S., Shariati, M., Ramli Sulong, N.H. and Tahir, M.M. (2016), "Shear capacity of C-shaped and L-shaped angle shear connectors", *Plos One*, **11**(8), e0156989. https://doi.org/10.1371/journal.pone.0156989.

Tan, L., Sun, Y., Wei, C., Tao, Y., Tian, Y., An, Y., Zhang, Y., Xiong, S. and Feng, J. (2021), "Design of robust, lithiophilic, and flexible inorganic-polymer protective layer by separator engineering enables dendrite-free lithium metal batteries with $LiNi_{0.8}Mn_{0.1}Co_{0.1}O_2$ cathode", *Small*, **17**(13), 2007717. https://doi.org/10.1002/smll.202007717.

Toghroli, A., Mohammadhassani, M., Suhatril, M., Shariati, M. and Ibrahim, Z. (2014), "Prediction of shear capacity of channel shear connectors using the ANFIS model", *Steel Compos. Struct.*, **17**(5), 623-639. http://doi.org/10.12989/scs.2014.17.5.623.

Toghroli, A., Suhatril, M., Ibrahim, Z., Safa, M., Shariati, M. and Shamshirband, S. (2016), "Potential of soft computing approach for evaluating the factors affecting the capacity of steel–concrete composite beam", *J. Intell. Manuf.*, 1-9. https://doi.org/10.1007/s10845-016-1217-y.

Toghroli, A., Shariati, M., Karim, M.R. and Ibrahim, Z. (2017), "Investigation on composite polymer and silica fume–rubber aggregate pervious concrete", *Proceedings of Fifth International Conference on Advances in Civil, Structural and Mechanical Engineering*, Zurich, Switzerland, September.

Toghroli, A., Shariati, M., Sajedi, F., Ibrahim, Z., Koting, S., Mohamad, E.T. and Khorami, M. (2018), "A review on pavement porous concrete using recycled waste materials", *Smart Struct. Syst.*, **22**(4), 433-440. https://doi.org/10.12989/sss.2018.22.4.433.

Toghroli, A., Mehrabi, P., Shariati, M., Trung, N.T., Jahandari, S. and Rasekh, H. (2020), "Evaluating the use of recycled concrete aggregate and pozzolanic additives in fiber-reinforced pervious concrete with industrial and recycled fibers", *Constr. Build. Mater.*, **252**, 118997. https://doi.org/10.1016/j.conbuildmat.2020.118997.

Trung, N.T., Shahgoli, A.F., Zandi, Y., Shariati, M., Wakil, K., Safa, M. and Khorami, M. (2019a), "Moment-rotation prediction of precast beam-to-column connections using extreme learning machine", *Struct Eng. Mech.*, **70**(5), 639-647. https://doi.org/10.12989/sem.2019.70.5.639.

Trung, N.T., Alemi, N., Haido, J.H., Shariati, M., Baradaran, S. and Yousif, S.T. (2019b), "Reduction of cement consumption by producing smart green concretes with natural zeolites", *Smart Struct. Syst.*, **24**(3), 415-425. https://doi.org/10.12989/sss.2019.24.3.415.

Tsai, Y.H., Wang, J., Chien, W.T., Wei, C.Y., Wang, X. and Hsieh, S.H. (2019), "A BIM-based approach for predicting corrosion under insulation", *Autom. Constr.*, **107**, 102923. https://doi.org/10.1016/j.autcon.2019.102923.

Wang, M., Wang, W.X., Chen, H.S. and Li, Y.L. (2018), "Understanding micro-diffusion bonding from the fabrication of B 4 C/Ni composites", *Int. J. Miner. Metall. Mater.*, **25**(3), 365-374. https://doi.org/10.1016/j.jmatprotec.2008.06.014.

Wei, X., Shariati, M., Zandi, Y., Pei, S., Jin, Z., Gharachurlu, S., Abdullahi, M.M., Tahir, M.M. and Khorami, M. (2018), "Distribution of shear force in perforated shear connectors", *Steel Compos. Struct.*, **27**(3), 389-399. http://doi.org/10.12989/scs.2018.27.3.389.

Whitelegg, J. and Cross, W. (1995), "Health of professional drivers a report for transport & general workers union", Research Report No. 00715974; Transport Research Laboratory, West Drayton, U.K.

Xu, M.X., Chen, Z.H. and Xu, M.Q. (2014), "Micro-mechanism of metal magnetic memory signal variation during fatigue", *Int. J. Miner. Metall. Mater.*, **21**(3), 259-265. https://doi.org/10.1007/s12206-016-0618-3.

Yang, Y., Chen, H., Zou, X., Shi, X.L., Liu, W.D., Feng, L., Suo, G., Hou, X., Ye, X. and Zhang, L. (2020a), "Flexible carbon-fiber/semimetal Bi nanosheet arrays as separable and recyclable plasmonic photocatalysts and photoelectrocatalysts", *ACS Appl. Mater. Interfac.*, **12**(22), 24845-24854. https://doi.org/10.1016/j.matchemphys.2021.124990.

Yang, Z., Xu, P., Wei, W., Gao, G., Zhou, N. and Wu, G. (2020b), "Influence of the crosswind on the pantograph arcing dynamics", *IEEE T. Plasma Sci.*, **48**(8), 2822-2830. https://doi.org/10.1109/TPS.2020.3010553.

Yazdani, M., Kabirifar, K., Frimpong, B.E., Shariati, M., Mirmozaffari, M. and Boskabadi, A. (2020), "Improving construction and demolition waste collection service in an urban area using a simheuristic approach: A case study in Sydney, Australia", *J. Clean. Prod.* **280**, 124138. https://doi.org/10.1016/j.jclepro.2020.124138.

Yin, P.F., Han, X.Y., Zhou, C., Xia, C.H., Hu, C.L. and Sun, L.L. (2015), "Large-scale synthesis of nickel sulfide micro/nanorods via a hydrothermal process", *Int. J. Miner. Metall. Mater.*, **22**(7), 762-769. https://doi.org/10.1007/978-3-319-63215-5_20.

Zandi, Y., Shariati, M., Marto, A., Wei, X., Karaca, Z., Dao, D., Toghroli, A., Hashemi, M.H., Sedghi, Y. and Wakil, K. (2018), "Computational investigation of the comparative analysis of cylindrical barns subjected to earthquake", *Steel Compos. Struct.*, **28**(4), 439-447. https://doi.org/10.12989/scs.2018.28.4.439.

Zhang, B., Ji, D., Fang, D., Liang, S., Fan, Y. and Chen, X. (2019), "A novel 220-GHz GaN diode on-chip tripler with high driven power", *IEEE Electr. Device L.*, **40**(5), 780-783. https://doi.org/10.1109/LED.2019.2903430.

Zhang, B., Niu, Z., Wang, J., Ji, D., Zhou, T., Liu, Y., Feng, Y., Hu, Y., Zhang, J. and Fan, Y. (2020a), "Four-hundred gigahertz broadband multi-branch waveguide coupler", *IET Microw. Antennas Propag.*, **14**(11), 1175-1179. https://doi.org/10.1049/iet-map.2020.0090.

Zhang, L., Zheng, J., Tian, S., Zhang, H., Guan, X., Zhu, S., Zhang, X., Bai, Y., Xu, P. and Zhang, J. (2020b), "Effects of Al3+ on the microstructure and bioflocculation of anoxic sludge", *J. Environ. Sci.*, **91**, 212-221. https://doi.org/10.1016/j.jes.2020.02.010.

Zhang, L., Zhang, M., You, S., Ma, D., Zhao, J. and Chen, Z. (2021), "Effect of Fe^{3+} on the sludge properties and microbial community structure in a lab-scale A^2O process", *Sci. Total Environ.*, **780**, 146505. https://doi.org/10.1016/j.scitotenv.2021.146505.

Zhang, X. and Zhang, Y. (2021), "Experimental study on enhanced heat transfer and flow performance of magnetic nanofluids under alternating magnetic field", *Int. J. Therm. Sc.*, **164**, 106897. https://doi.org/10.1016/j.ijthermalsci.2021.106897.

Zhao, Y., Moradi, Z., Davoudi, M. and Zhuang, J. (2021), "Bending and stress responses of the hybrid axisymmetric system via state-space method and 3D-elasticity theory", *Eng. Comput.*, 1-23. https://doi.org/10.1007/s00366-020-01242-1.

Zhu, Q. and Ishitobi, M. (2004), "Chaos and bifurcations in a nonlinear vehicle model", *J. Sound Vib.*, **275**(3-5), 1136-1146. https://doi.org/10.1016/j.ijsolstr.2005.06.070.

Zhu, Q. and Ishitobi, M. (2006), "Chaotic vibration of a nonlinear full-vehicle model", *Int. J. Solids Struct.*, **43**(3-4), 747-759. https://doi.org/10.1016/j.ijsolstr.2005.06.070.

Zhu, H., An, Y., Shi, M., Li, Z., Chen, N., Yang, C. and Xiao, P.

(2021), "Porous N-doped carbon/MnO_2 nanoneedles for high performance ionic liquid-based supercapacitors", *Mater. Lett.*, **296**, 129837. https://doi.org/10.1016/j.matlet.2021.129837.

Ziaei-Nia, A., Shariati, M. and Salehabadi, E. (2018), "Dynamic mix design optimization of high-performance concrete", *Steel Compos. Struct.*, **29**(1), 67-75. http://doi.org/10.12989/scs.2018.29.1.067.

AT